Письма в ЭЧАЯ. 2005. Т. 2, № 2(125). С. 72–81

УДК 539.126+539.126.3

SIMULATION OF $\phi \to K^+K^-$ DETECTION IN THE ALICE EXPERIMENT

B. Batyunya [a], *A. De Caro* [b], *G. Paić* [c], *A. Pesci* [b], *S. Zaporozhets* [a]
(for the ALICE collaboration)

[a] Joint Institute for Nuclear Research, Dubna
[b] Dipartimento di Fisica dell'Universita and Sezione INFN, Bologna, Italy
[c] CERN, Geneva

Simulation studies on the K^+K^--pair production and detection in the ALICE detector for Pb–Pb collisions at the LHC energy were performed. The possibility of selecting a ϕ-meson signal over the combinatorial background in the different transverse momentum regions is demonstrated using the realistic simulation tracking and particle identification programs in the ALICE offline framework (AliRoot).

Выполнено моделирование образования и регистрации K^+K^--пар в эксперименте ALICE для Pb–Pb-взаимодействий при энергии LHC. Продемонстрирована возможность выделения сигнала ϕ-мезона над комбинаторным фоном в различных областях поперечного импульса с использованием программ реалистичного моделирования восстановления треков и идентификации частиц в рамках общего пакета программной обработки в эксперименте ALICE (AliRoot).

INTRODUCTION

The production of vector mesons and strange particles is expected to provide detailed information on the reaction dynamics of ultra-relativistic nucleus–nucleus collisions [1, 2]. The ϕ meson is of particular interest due to its $(s\bar{s})$ valence quark content, which makes the ϕ a signature of strangeness production mechanism from a possible early partonic phase [2, 3]. The enhancement of ϕ production was proposed [4] as a quark-gluon plasma (QGP) signature in nucleus–nucleus collisions. Shifts of the ϕ-meson mass and changes in its line-shape in a hot hadronic medium have been predicted [5]. The production rate and the partial decay width into kaons may change as a consequence of partial chiral symmetry restoration [6].

The ϕ decay will be observed in ALICE (A Large Ion Collider Experiment, [7]) in both lepton and kaon channels, and the ratio of the decay widths in these two channels might be very sensitive to changes in parton or kaon masses [8]. The recent SPS Pb–Pb [9] and RHIC Au–Au [10, 11] results show that no change of the mass or width is observed at SPS and RHIC energies. But, at the same time, a rise of the slope parameter by a factor of 1.7 in the transverse spectra and an enhancement of the ϕ/π ratio by a factor of 3 as compared to the minimum-bias $p + p$ interactions were found [9, 12].

The main experimental problem to select the hadronic mode of ϕ decays in heavy-ion interactions at the LHC energy is a very high combinatorial background. For example, the HIJING model [13] predicts in the pseudo-rapidity window of $-1 \leqslant \eta \leqslant 1$ for the central

Pb–Pb events the number of primary charged kaons about 1500, which is 15 times larger than the number of kaons from ϕ decays (see below). It is clear that in such conditions we require the optimal particle identification and the kinematic regions with the best signal-to-background ratio (S/B). The preliminary simulation of the expected experimental mass spectrum of K^+K^- pairs and $\phi \to K^+K^-$ decay detection in ALICE were reported in [14] (see also Section 11.4.3 in [7]), where the different kinematic cuts have been studied based on the fast simulation to improve the S/B value. Here we present results obtained in the framework of the AliRoot [15] simulation package making use of C++ as a language and ROOT as a framework. All detector efficiencies were calculated using the new detailed simulation programs and the realistic tracking package was used to get the tracking efficiencies, momentum and angular resolutions and particle identification (PID) efficiencies.

The simulation was performed for two different classes of events: in the full transverse momentum region and for particles with $p_t > 1.5$ GeV/c (high transverse momentum region).

1. SIMULATION METHOD

1.1. Full Transverse Momentum Region. The general simulation method consisted of two steps:

• detailed simulations of the detectors, tracking and kaon PID to calculate the necessary efficiencies and momentum and angle resolutions for the reconstructed tracks,

• fast simulation of K^+K^--pair detection and analysis using the efficiencies and track resolutions obtained at the first step.

The detailed simulation of the Inner Tracking System (ITS, [16]) and the Time Projection Chamber (TPC, [17]) were used for the tracking. The TPC and the Time of Flight (TOF, [18]) were used for kaon identification at the first step. It should be noted that to perform the PID in the TOF the detailed simulation of the detector itself has been done, but the particle momenta were taken from the GEANT information, i.e., without using ITS–TPC tracking. About 250 full HIJING [13] events were processed in the ITS, TPC and TOF acceptance (in the full azimuthal angle (ϕ) range and in the pseudo-rapidity (η) range of $-1 \leqslant \eta \leqslant 1$). The charged particle density ($dN_{\rm ch}/d\eta$ at $\eta = 0$) is about 6000 for Pb–Pb collisions at LHC energy with 10% of charged kaon production. The magnetic field of 0.4 T was used. The full efficiency as a function of the transverse momentum (p_t) and η have been extracted for charged kaons. We mean by the «full efficiency» the ratio of the number of identified kaons to the generated ones. This means that the full efficiency takes into account the losses during the detection, tracking and PID.

The p_t dependence of the transverse momentum and angle resolutions were determined during the simulation.

Figure 1, a–d shows the dependences of the full kaon efficiency on p_t in the different η regions for the TPC. The low efficiencies at lower momentum are mostly due to kaon decays and tracking inefficiency, which in turn is a consequence of the short particle path inside the TPC because of the track curling in the magnetic field. The high-p_t limit of the kaon selection is a consequence of the TPC PID limit since the signals from pions and kaons overlap each other in the momentum region of $0.6 \div 0.7$ GeV/c (see, for example, Fig. 11.18 in [7]).

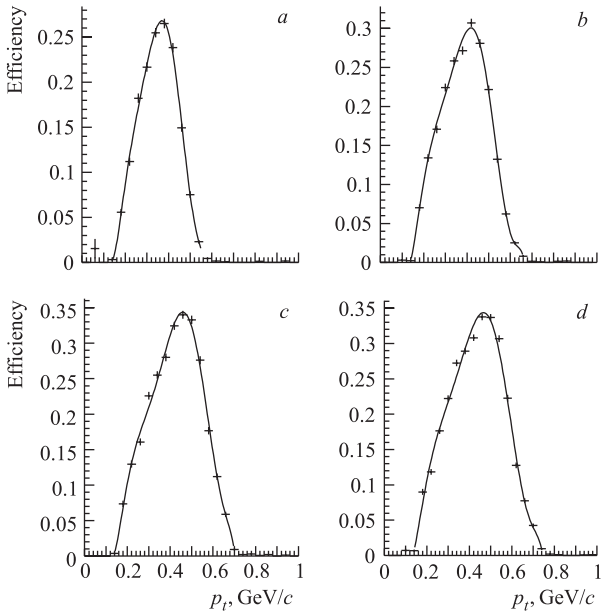

Fig. 1. Dependences of full kaon efficiency (see text) on p_t in the different pseudo-rapidity (η) regions for the TPC: *a*) $0.7 < |\eta| < 0.9$; *b*) $0.5 < |\eta| < 0.7$; *c*) $0.3 < |\eta| < 0.5$; *d*) $|\eta| < 0.3$. The curves are the results of the polynomial fits

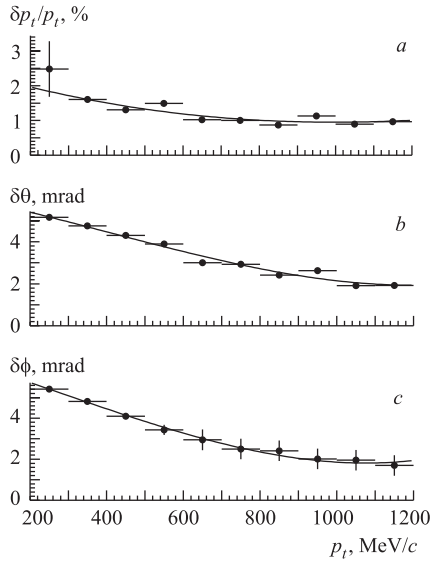

Fig. 2. Transverse momentum relative resolution $\delta p_t/p_t$ (*a*) and θ- and ϕ-angle resolutions (b, c) versus p_t for kaon tracks reconstructed in the ITS and TPC in the p_t region of $0.2 \div 1.2$ GeV/c. The curves are the results of polynomial fits

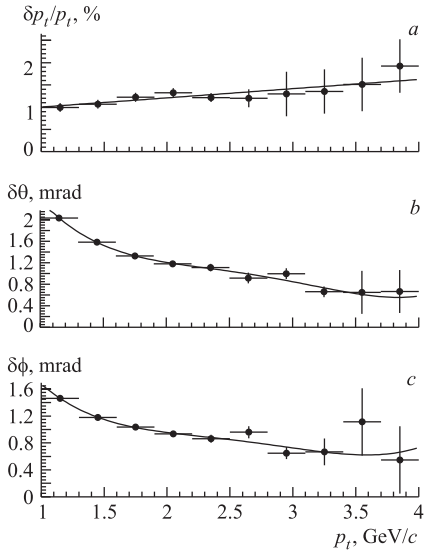

Fig. 3. The same dependences as in Fig. 2 but in the p_t region of $1.0 \div 4.0$ GeV/c

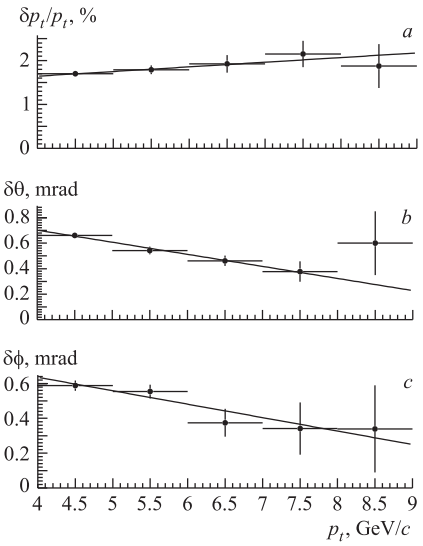

Fig. 4. The same dependences as in Fig. 2 but in the p_t region of $4.0 \div 9.0$ GeV/c

The relative p_t resolution and angular resolutions versus p_t are shown in Figs. 2–4 for different transverse momentum regions. One can see that in the p_t region of $0.2 \div 9.0$ GeV/c the relative p_t resolution is between $1.0 \div 2.0\%$ and the angular resolutions decrease from 5.0 to 0.3 mrad for both polar (θ) and azimuthal (ϕ) angles.

Figure 5, a–d shows the dependence of the full TOF efficiency for charged kaons on the p_t in different η regions (same as in Fig. 1, a–d, respectively). It is seen from Figs. 1 and 5 that the maximum full efficiency does not exceed $35 \div 40\%$ for both TPC and TOF. Figures 1 and 5 show also that the kaon identification regions of the TPC and TOF overlap in the interval of $p_t = 0.35 \div 0.75$ GeV/c.

AliGenParam generator of AliRoot has been used in the second fast simulation step with the possibility of generation arbitrary number of different type of particles having the uniform pseudo-rapidity distribution in the acceptance under study ($-1 \leqslant \eta \leqslant 1$) and exponential p_t distribution (see below). The decays of the particles are performed using the PYTHIA generator [19]. To combine the generation both of charged kaons and of $\phi \to K^+K^-$ decays, the AliGenCocktail generator (also in AliRoot) has been used, which allows us to combine arbitrary number of any particle types. This number of charged kaons and ϕ decays in the acceptance was estimated from charged pion multiplicity (9000 $\pi^{\pm}$ taken from the HIJING) and using the particle ratios K/π and ϕ/π obtained in the SPS [9, 12, 20] and RHIC [11, 21] experimental data. As a result, 1500 charged kaons and 55 $\phi \to K^+K^-$ decays have been generated per event on average in the acceptance of the detectors.

Figure 6 shows the generated distribution of $m_t - m_0$ for kaons and ϕ mesons, where m_t and m_0 are the transverse and particle masses, respectively. The lines are fit results by the function $\exp(-(m_t - m_0)/T)$ with $T = 480$ MeV for ϕ and $T = 309$ and 390 MeV for the first and second slopes, respectively, of the distribution for kaons. We note that the values for

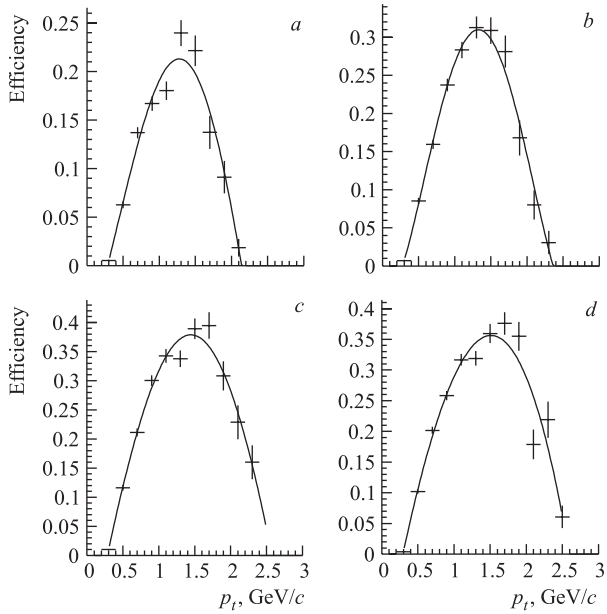

Fig. 5. Dependence of full kaon efficiency (see text) on p_t in the different pseudo-rapidity (η) regions for TOF: *a*) $0.7 < |\eta| < 0.9$; *b*) $0.5 < |\eta| < 0.7$; *c*) $0.3 < |\eta| < 0.5$; *d*) $|\eta| < 0.3$. The curves are the results of the polynomial fits

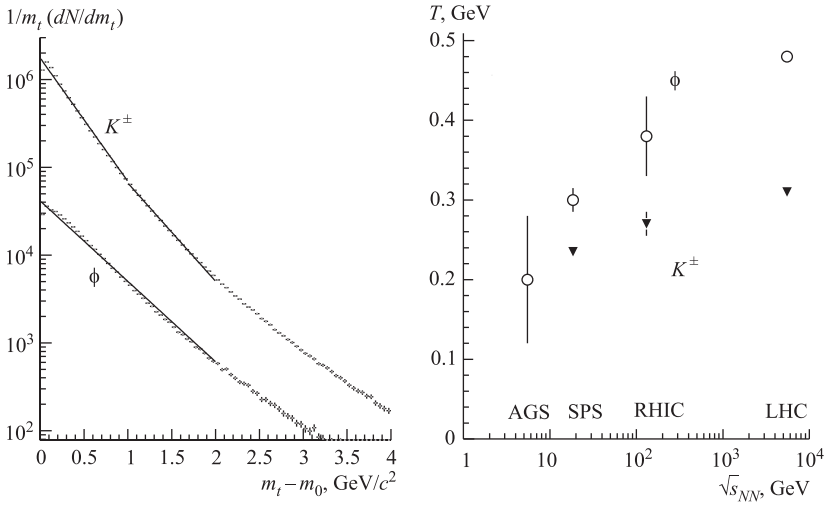

Fig. 6. The m_t spectra for kaons and ϕ obtained by AliGenParam generator. The curves are the results of exponential fits

Fig. 7. Dependences of the slope parameter T (see text) on energy in c.m.s. per nucleon for ϕ at $(m_t - m_0) < 2$ GeV/c^2 (circles) and charged kaon at $(m_t - m_0) < 1$ GeV/c^2 (triangles) production in different experiments (AGS, SPS, RHIC). The LHC points have been obtained by the simulation using AliGenParam generator (see text)

T are higher than those obtained at the AGS [22], SPS [9,23] and RHIC [11,21] experiments for the central events, and this excess tendency corresponds to the rise of this parameter with energy, as is seen in Fig. 7.

Next, kaons have been identified taking into account the TPC and TOF efficiencies separately for each kaon using the polynomial fits (the curves in Figs. 1 and 5). We note that we increase the number of the found ϕ's by 20%, using different detectors for the identification of the two decay products. We have not taken into account $5 \div 7\%$ of the pion and proton contamination to the kaon sample in this simulation.

The p_t and angles of the K^+ and K^- were smeared by Gaussian distributions with a sigma equal to the resolutions obtained from the fits (the curves in Figs. 2 and 3) and then the new p_x, p_y, p_z components have been applied to calculate the effective mass of K^+K^- pairs.

1.2. High Transverse Momentum Region. To study the detection of ϕ mesons and background K^+K^- pairs in the high-p_t region, $p_t > 1.5$ GeV/c for each particle, a special simulation was performed without any particle identification. Again, the AliGenParam and AliGenCocktail generators were used to generate pions, kaons, protons, antiprotons and ϕ resonances. We have taken for the full p_t region the numbers of $\pi^{\pm}$, $K^{\pm}$ and ϕ decays presented in Subsec. 1.1 and the numbers of protons and antiprotons from $\bar{p}/\pi^-$ and $\bar{p}/p$ ratios obtained in the STAR experiment [24,25]. We determined the number of each particle type in the high-p_t region ($p_t > 1.5$ GeV/c), and, as a result, 320 charged pions, 160 charged kaons, 200 protons and antiprotons and 18 $\phi \to K^+K^-$ decays have been generated per event on the average.

Again, the momentum components were smeared according to the relative p_t and angular resolution functions shown in Figs. 3 and 4.

2. RESULTS

2.1. Full Transverse Momentum Region. Figure 8, a shows the K^+K^- effective-mass spectrum obtained from 10^6 cocktail generator events at $p_t(K^+K^-) > 2.2$ GeV/c. The ϕ

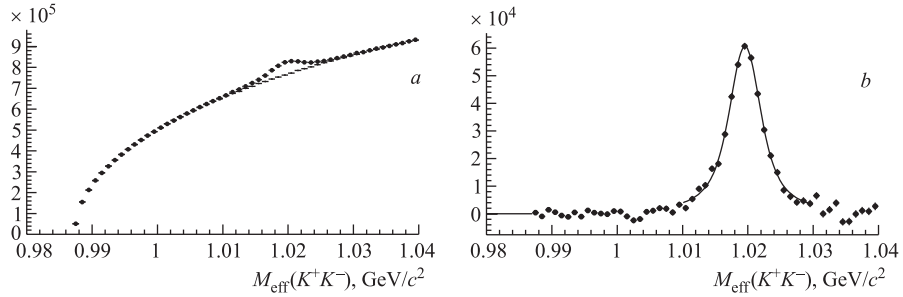

Fig. 8. *a*) Spectrum of K^+K^- effective mass in K^+K^--pair transverse momentum region of $\geqslant 2.2$ GeV/c. The K^+K^+ background distribution is also shown. *b*) Signal of ϕ meson after subtraction of the background. The curve is the Breit–Wigner fit result taking into account the effective-mass resolution (see text)

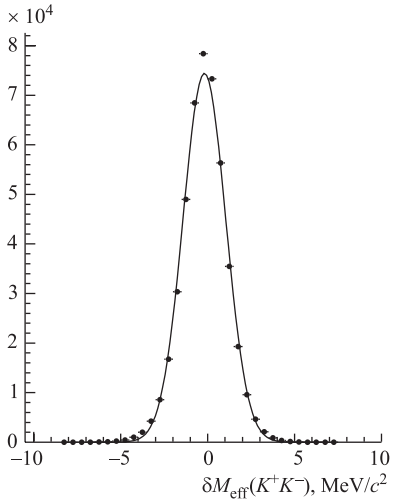

Fig. 9. K^+K^- effective-mass resolution at $p_t(K^+K^-) > 2.2$ GeV/c. The curve is the fit result by the Gaussian function

signal is clearly seen over the combinatorial background obtained for K^+K^+ pairs. Figure 8, b shows the ϕ signal found after subtraction of this combinatorial background. To extract the resonance width, it is necessary to take into account the effective-mass resolution. Figure 9 shows the distribution of the differences of the effective masses obtained with and without track momentum and angle smearing by the respective Gaussian functions. The curves are the Gaussian fit results with the parameter $\sigma = 1.23$ MeV/c^2. This σ value (the effective-mass resolution) has been taken for a convolution of the Breit–Wigner and Gaussian functions using for the K^+K^- effective-mass approximation. The result is shown in the effective-mass region $1.01 \div 1.03$ GeV/c^2 by the curve in Fig. 8, b with the mass and width of the ϕ resonance (1019.60 ± 0.04) MeV/c^2 and (4.43 ± 0.12) MeV/c^2, respectively. One can see that these values are consistent with the PDG ones used in the generation code.

Table 1 presents the S/B and the significance $(S/\sqrt{B+S})$ in the different p_t regions of the K^+K^- pairs. The signal (S) is presented as well. One can see that the S/B improves from 0.5% at the lowest p_t to 6.2% at the highest p_t and the significance is 120 for $p_t > 2.2$ GeV/c.

Table 1. **Signal number (S), signal-to-background ratio (S/B) and significance ($S/\sqrt{S+B}$) for the ϕ resonance in the region equal to one PDG width of the ϕ around the central mass bin at different p_t of the K^+K^- pairs**

p_t, GeV/c	S	S/B	$S/\sqrt{B+S}$
$\leqslant 0.6$	69435	0.005	18
0.6–0.8	253120	0.006	40
0.8–1.0	354150	0.008	55
1.0–1.2	264470	0.011	54
1.2–1.4	174745	0.014	50
1.4–1.6	124715	0.018	47
1.6–1.8	96395	0.023	46
1.8–2.0	83420	0.028	48
2.0–2.2	72870	0.035	49
> 2.2	253920	0.062	120

2.2. High Transverse Momentum Region. The results of the analysis at the high-p_t region without any particle identification are presented in Table 2 for 10^6 events. The S/B value increases from 1.0 to 20% at the $p_t(K^+K^-) \geqslant 7.5$ GeV/c, and the significance is about 50 at this maximum transverse momentum.

Figure 10, a shows the K^+K^- effective-mass distribution for $p_t(K^+K^-) > 7.5$ GeV/c and the K^+K^+ background. Figure 10, b shows the signal after background subtraction.

Table 2. **The same as in Table 1 but at high p_t of K^+K^- pairs**

p_t, GeV/c	S	S/B	$S/\sqrt{B+S}$
> 3.0	730630	0.012	95
> 3.5	586230	0.015	94
> 4.0	374480	0.022	89
> 4.5	223830	0.033	85
> 5.0	136950	0.048	80
> 5.5	86150	0.069	75
> 6.0	55860	0.097	70
> 6.5	35610	0.130	64
> 7.0	23150	0.170	57
> 7.5	15010	0.200	51

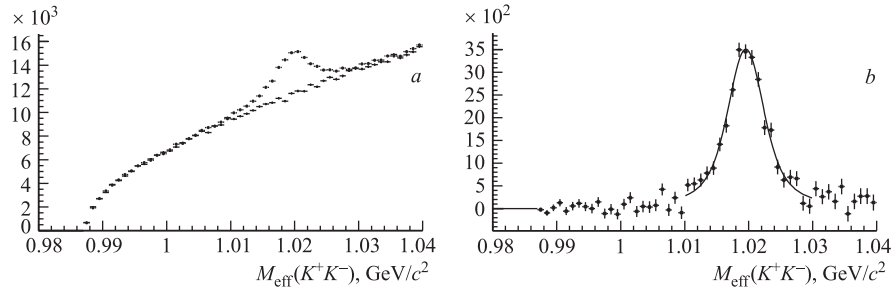

Fig. 10. *a*) Spectrum of K^+K^- effective mass at $p_t(K^+K^-) > 7.5$ GeV/c obtained without any particle identification. The K^+K^+ background distribution is also shown. *b*) Signal of ϕ meson after subtraction of the background. The curves are the Breit–Wigner fit result taking into account the effective-mass resolution (see text)

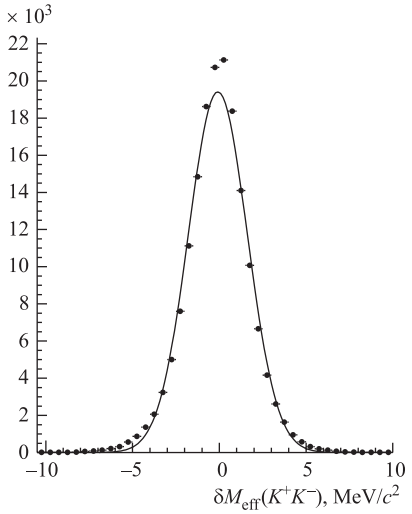

Fig. 11. K^+K^- effective-mass resolution at $p_t(K^+K^-) > 7.5$ GeV/c. The curve is the fit result by the Gaussian function

Again, to take into account the K^+K^- effective-mass resolution, the difference of the effective masses obtained with and without track momentum and angle smearing by the respective Gaussian functions were studied. Figure 11 shows a distribution of this mass difference at $p_t(K^+K^-) > 7.5$ GeV/c. The curve is the Gaussian fit result with $\sigma = 1.7$ MeV/c^2.

The curve in Fig. 10, b is the Breit–Wigner fit result in the effective-mass region $(1.01 \div 1.03)$ GeV/c^2 taking into account the effective-mass resolution (the convolution of the Breit–Wigner and Gaussian functions). The fit parameters, the mean mass and width, are (1019.56 ± 0.09) MeV/c^2 and (4.51 ± 0.27) MeV/c^2, respectively.

These values again close the PDG ones used in the generation code.

CONCLUSIONS

Simulation studies of the ϕ signal in the ALICE experiment (for Pb–Pb central events at LHC energy) were performed based on a high statistics sample of 10^6 events. The ITS, TPC and TOF simulations were used for the tracking and kaon identification for particle with $p_t < 2.5$ GeV/c and a magnetic field of 0.4 T. The signal-to-background ratio (S/B) in this case increases from 0.5% at the lowest p_t of K^+K^- pairs ($\leqslant 0.6$ GeV/c) by an order of magnitude at the highest p_t of K^+K^- ($\geqslant 2.2$ GeV/c). For ten p_t bins the largest significance ($S/\sqrt{S+B}$) reaches the value of 120 standard deviations (for the best S/B value).

A special simulation was performed for the high-p_t region where transverse momentum of each particle is larger than 1.5 GeV/c without any particle identification. The largest S/B is 20% at the $p_t(K^+K^-) > 7.5$ GeV/c with significance of about 50.

In both simulations the Breit–Wigner fits of the signals, taking into account the effective-mass resolution, lead to ϕ-meson mass and width values that are very near to the PDG ones used in the generator. For example, the width coincides with the natural width within one standard deviation. Therefore, we may be sensitive to possible in-medium modification of the ϕ width down to 1.5÷3.0 MeV/c^2.

REFERENCES

1. *Hatsuda T., Kunihiro T.* // Phys. Rep. 1994. V. 247. P. 221.
2. *Koch P. et al.* // Phys. Rep. 1986. V. 142. P. 167.
3. *Rafelski J., Muller B.* // Phys. Rev. Lett. 1982. V. 48. P. 1066;
   Bass S. A. et al. // Nucl. Phys. A. 1999. V. 661. P. 205.
4. *Shor A.* // Phys. Rev. Lett. 1985. V. 54. P. 1122.
5. *Asakawa M., Ko C. M.* // Nucl. Phys. A. 1994. V. 572. P. 732.
6. *Pisarski R. D., Wilczek F.* // Phys. Rev. D. 1984. V. 29. P. 338;
   Shuryak E. V. // Nucl. Phys. A. 1991. V. 525. P. 3c.
7. *ALICE Collab.* Technical Proposal. CERN/LHCC 95-71. LHCC/P3. 1995.
8. *Johnson S. C. et al.* // Phys. J. C. 2001. V. 18. P. 645.

9. *Afanasiev S. V. et al.* // Phys. Lett. B. 2000. V. 491. P. 59.

10. *Zhangbu Xu* // Nucl. Phys. A. 2002. V. 698. P. 607c.

11. *Adler C. et al.* // Phys. Rev. C. 2002. V. 65. P. 041901(R).

12. *Friese V.* // Nucl. Phys. A. 2002. V. 698. P. 487c.

13. *Wang N. X. et al.* // Phys. Rev. D. 1991. V. 44. P. 3521; Phys. Rev. Lett. 1992. V. 68. 1480.

14. *Batyunya B. et al.* // JINR Rapid Commun. 1997. No.5[85]. P. 61; Internal Note/SIM ALICE/97-26. 1997.

15. *ALICE Collab.* Physics Performance Report. CERN/LHCC 2003-049, ALICE PPR. 2003. V. 1.

16. *ALICE Collab.* Inner Tracking System. Technical Design Report. CERN/LHCC 99-12, ALICE TDR 4. 1999.

17. *ALICE Collab.* Time Projection Chamber. Technical Design Report. CERN/LHCC 2000-001, ALICE TDR 7. 2000.

18. *ALICE Collab.* Time of Flight System. Technical Design Report. CERN/LHCC 2000-12, ALICE TDR 8. 2000; *ALICE Collab.* Time of Flight System. Technical Design Report, Addendum. CERN/LHCC 2002-016, Addendum to ALICE TDR 8. 2002.

19. *Sjöstrand T.* // Comp. Phys. Commun. 1994. V. 82. P. 74.

20. *Afanasiev S. V.* // Nucl. Phys. A. 2002. V. 698. P. 104c.

21. *Caines H.* // Ibid. P. 112c.

22. *Seto R. K. et al.* // Nucl. Phys. A. 1999. V. 661. P. 506c.

23. *Bearden I. G. et al.* // Phys. Rev. Lett. 1997. V. 78. P. 2080.

24. *STAR Collab.* // Phys. Rev. Lett. 2001. V. 86. P. 4778.

25. *Harris J.* (*STAR Collab.*). Talk presented at QM2001, Stony Brook, Jan. 2001.

Received on May 13, 2004.